Analysis of Creep Rupture Behavior of Cr-Mo Ferritic Steels in the Presence of Notch

SUNIL GOYAL, K. LAHA, C.R. DAS, and M.D. MATHEW

Effect of notch on creep rupture behavior of 2.25Cr-1Mo, 9Cr-1Mo, and modified 9Cr-1Mo ferritic steels has been assessed. Creep tests were carried out on smooth and notched specimens of the steels in the stress ranging 90 to 300 MPa at 873 K (600 °C). Creep rupture lives of the steels increased in the presence of notch over those of smooth specimens, thus exhibiting notch strengthening. The strengthening was comparable for the 9Cr-1Mo and 2.25Cr-1Mo steels and appreciably more in modified 9Cr-1Mo steel. The strengthening effect was found to decrease with the decrease in applied stress and increase in rupture life for all the steels. The presence of notch decreased the creep rupture ductility of the steels significantly and the 2.25Cr-1Mo steel suffered more reduction than in the other two 9Cr-steels. Finite element analysis of stress distribution across the notch was carried out to understand the notch strengthening and its variation in the steels. The variation in fracture appearance has also been corroborated based on finite element analysis. Reduction in von-Mises stress across the notch throat plane resulted in strengthening in the steels. Higher reduction in von-Mises stress in modified 9Cr-1Mo steel than that in 2.25Cr-1Mo and 9Cr-1Mo steels induced more strengthening in modified 9Cr-1Mo steel under multiaxial state of stress.

DOI: 10.1007/s11661-014-2609-2

I. INTRODUCTION

GOOD thermophysical properties, high-temperature oxidation resistance, and mechanical properties and cost effectiveness compared to austenitic stainless steels are the main reasons for selection of ferritic steels as a structural material for steam generating systems of nuclear power plants, fossil-fired power plants, and petrochemical industries. The Cr-Mo ferritic steels derive their high-temperature strength from the solid solution strengthening, phase-transformation-induced dislocation substructure, and intra- and inter-granular metal-carbonitride precipitates. Extensive studies have been carried out on uniaxial creep behavior of these steels and their weld joints.[1–3] However, the components often experience multiaxial state of stress either due to change in geometry or mode of loading during service. In order to assess the life of such components, it is important to estimate the deformation and damage behavior of the components under multiaxial state of stress. Notched specimens are widely used to study the effect of multiaxial state of stress on creep deformation and rupture behavior of materials.[4–11]

SUNIL GOYAL, Scientific Officer, K. LAHA, Head, Creep Studies Section, and M.D. MATHEW, Head, are with the Mechanical Metallurgy Division, Metallurgy and Materials Group, Indira Gandhi Centre for Atomic Research, Kalpakkam 603 102, India. Contact e-mail: goyal@igcar.gov.in C.R. DAS, Scientific Officer, is with the Materials Technology Division, Metallurgy and Materials Group, Indira Gandhi Centre for Atomic Research.

Manuscript submitted February 3, 2014.
Article published online October 10, 2014

The presence of notches may result in notch strengthening or weakening depending on the notch shape and sharpness, testing conditions and the material.[7–11] Notch strengthening is expected when the high axial stresses across the notch throat plane redistribute quickly to a level below the applied stress. This kind of behavior is typically observed in ductile materials. However, the notch weakening is expected in situations where the very high axial stresses due to the presence of notch redistribute very slowly, and the local accumulated strain exceeds the limit which is required for fracture before attaining the steady state across the notch root.

The stresses around the notch redistribute during creep deformation and approach to a steady-state condition.[12–15] Finite element (FE) analysis has been extensively used for estimating stress distribution and damage evolution around the notches under creep conditions.[12–14] The FE analysis was carried out to study the effect of different parameters *viz*. notch geometry, notch acuity, and material's ductility on stress redistribution in notched specimens by Eggeler *et al*.[15] The redistribution of the stresses was found to be dependent on the creep constitutive law obeyed by the material. Extensive information on uniaxial creep behavior of the materials exists in open literature; however, limited work has been carried out on multiaxial creep behavior.[16–18]

Creep deformation in materials leads to creep cavitation which is appreciably affected by the state of stress.[19–21] Creep cavitation in materials proceeds with the nucleation of creep cavities and their growth followed by linkage into discrete cracks leading to failure. Nucleation of creep cavity in Cr-Mo ferritic

steels under multiaxial state of stress has been discussed by Cane,[22] Goyal *et al.*[23] and Perrin *et al.*[24] Creep deformation of the matrix is associated with the grain boundary sliding (GBS) especially at relatively higher homologous temperature (T/T_m), where T is the test temperature and T_m is the melting point of the material. The inhomogeneous grain boundary sliding around the grain boundary irregularities, such as grain boundary triple point, ledges, particles, *etc*., induces stress concentration around them, leading to the nucleation of intergranular creep cavities. The von-Mises stress plays a dominant role in the nucleation of creep cavities resulted from decohesion of grains across the boundaries. Grain boundary sliding is expected to dominate over the creep deformation at relatively lower stresses and higher creep rupture lives. Bano *et al*., based on the detailed accommodation mechanisms of GBS, predicted wedge-type cracking below $0.5T/T_m$ and r-type creep cavitation at higher temperatures in Cr-Mo steels.[25,26] Hsia *et al*. carried out numerical study considering the effect of GBS on the creep damage.[27] The model was further extended for the multiaxial state of stress.[28] The creep deformation, grain boundary sliding, and damage depend on the test temperature appreciably. The stress distribution under multiaxial state of stress is expected to depend on test temperature, significantly affecting the creep cavitation. The growth of nucleated cavities strongly depends on the maximum principal and hydrostatic components of the stress.

In the present investigation, effect of notch on creep behavior of different Cr-Mo steels has been studied. The steels studied are 2.25Cr-1Mo, 9Cr-1Mo, and modified 9Cr-1Mo steels. The steels are extensively used in power plants and petrochemical industries. Steady-state FE analysis has been carried out to estimate the stresses across the notch throat plane. The variation in fracture behavior and strengthening effect has been correlated based on the distribution of stresses across the notch.

II. EXPERIMENTAL

A. *Materials and Creep Experiments*

In the present investigation, creep behavior of three ferritic steels *viz*. 2.25Cr-1Mo, 9Cr-1Mo, and modified 9Cr-1Mo steel in the presence of notch has been studied. Chemical composition of the steels used in this study is given in Table I. The 12-mm-thick plates were received in normalized and tempered heat treated condition. The 2.25Cr-1Mo, 9Cr-1Mo, and modified 9Cr-1Mo steels were normalized at 1223 K (950 °C) for 15 minutes, 1223 K (950 °C) for 15 minutes, and 1313 K (1040 °C) for 1 hour, respectively, whereas the steels were tempered at 1003 K (730 °C) for 60 minutes, 1053 K (780 °C) for 120 minutes, and 1033 K (760 °C) for 1 hour. In the normalized and tempered condition, the 2.25Cr-1Mo steel had tempered bainitic structure, whereas the 9Cr-1Mo and modified 9Cr-1Mo steels had tempered martensitic structure. Prior austenite grain sizes of the steels were 28, 24, and 23 μm, respectively, for 2.25Cr-1Mo, 9Cr-1Mo, and modified 9Cr-1Mo steels.

Creep tests were carried out on smooth and notched specimens of the steels at different stresses ranging from 90 to 230 MPa at 873 K (600 °C). Considering the expected stress concentration in notched specimens, the creep tests on smooth specimens of the steels have been carried out at higher stresses (up to 300 MPa) to facilitate the FE analysis. The applied stresses were calculated based on the minimum cross section in notched specimen. Circumferentially U-notch with notch root radii of 1.25 mm, keeping the minimum diameter of the specimen constant (5 mm), similar to smooth specimen, was introduced in the cylindrical specimens of the steels, Figure 1. The ratio of diameter of parallel portion of specimen to notch throat diameter (D/d) was fixed at 1.67.[29] Two notches were provided in each specimen so that the un-failed notch could be utilized for post-creep test metallographic investigations. The notches were sufficiently apart (≈20 mm) to avoid the interference of stress fields between them.[30] Tests on notched specimens were carried out in such a way that net applied stress acting in the notch throat plane was equal to the nominal stress on smooth specimen. Tensile tests were also carried out on the steels to incorporate the elastic–plastic behavior of the steels in FE analysis.

Electron Back Scatter Diffraction (EBSD) studies were carried out to understand the difference in deformation behavior of the steels under multiaxial state of stress. For EBSD studies, the un-broken notch region of the failed specimens was extracted and mechanically polished. Finally, the specimens were polished using colloidal suspension silica. EBSD measurements were

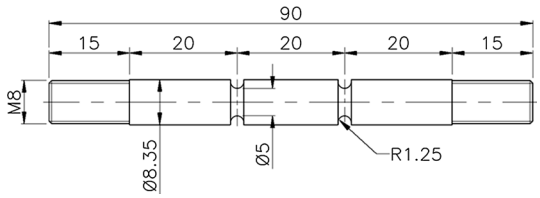

Fig. 1—Geometry of creep specimen used for the investigation (all dimensions are in mm).

Table I. Chemical Composition of the Steels (Weight Percent)

Material\Element	C	Si	Mn	P	S	Cr	Mo	V	Nb	N	Fe
2.25Cr-1Mo Steel	0.06	0.18	0.48	0.008	0.008	2.18	0.93	—	—	—	bal.
9Cr-1Mo Steel	0.1	0.49	0.46	0.008	0.002	8.36	0.93	—	—	—	bal.
Mod. 9Cr-1Mo Steel	0.092	0.39	0.45	<0.005	0.004	8.8	0.93	0.23	0.08	0.033	bal.

conducted using SEM equipped with an EBSD-system operating at an accelerating voltage of 20 kV with the pre-tilted stage at 70 deg with respect to horizontal axis. KHL software was used for the data acquisition and analysis. The scans were performed with a scan step size of 0.3 μm at two different locations of the notched specimens *viz*., center and root of the notch.

B. *Finite Element Analysis*

Finite element analysis of stress distribution across the notch throat plane during creep exposure was carried out to understand creep rupture behavior of the notched specimens. Finite element analysis was carried out considering both the 2D and 3D geometries of the notched specimen employing ABAQUS 6.10 finite element package. The typical mesh used for the notched specimen geometries for 2D and 3D analysis is shown in Figures 2(a) and (b), respectively. The 2D axisymmetric analysis was carried out using 4-noded quadrilateral elements, whereas the 3D analysis was carried out using 4-noded C3D4 tetrahedron elements.

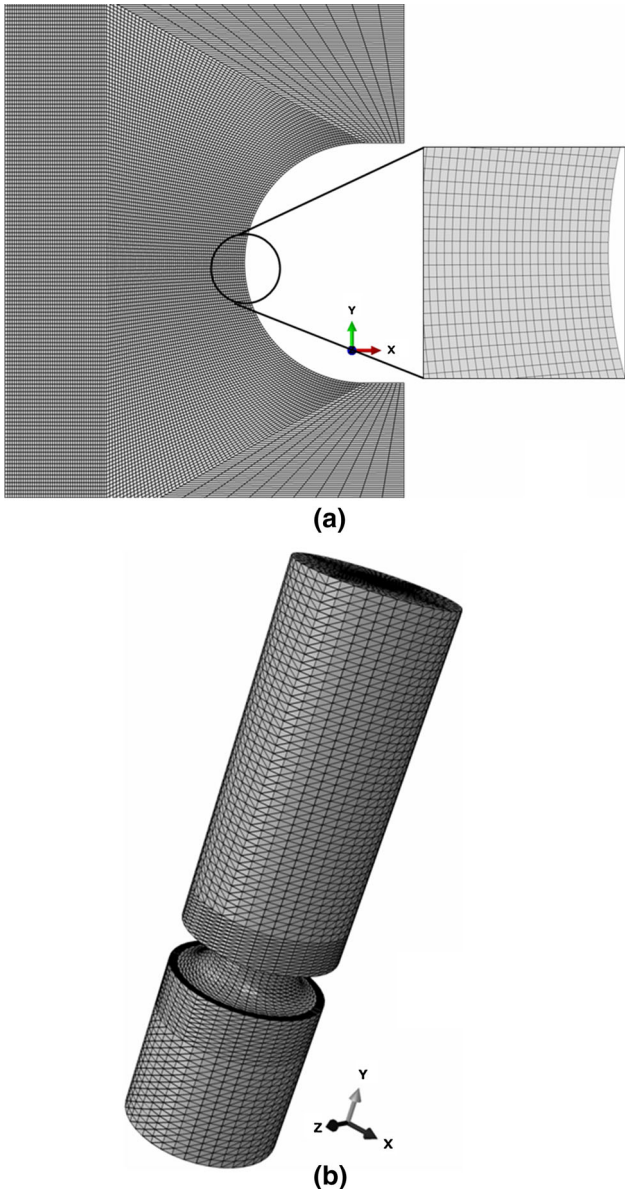

Fig. 2—Typical mesh used for (*a*) 2D and (*b*) 3D FE analysis of stress distribution across the notched specimen.

The analysis was carried out implementing elastic–plastic-creep behavior of the materials. The elastic–plastic behavior was incorporated in the model using Hollomon equation ($\sigma_t = K\varepsilon_p^{n'}$) relating true stress with true plastic strain and creep behavior using Norton's creep law relating the steady-state creep rate with applied stress ($\dot{\varepsilon}_s = A\sigma^n$). The experimentally determined constants of the constitutive equations for the steels under investigation are shown in Table II.

Von-Mises yield criterion has been used for occurrence of yielding in the steels. The material was assumed to deform elastically or elastic-plastically depending on the notch root radius and net applied stress initially, followed by creep deformation. The element size was reduced at and close to the notch root, and elastic analysis was used to ensure that the mesh configuration was sufficiently refined near the notch root to predict the theoretical elastic stress concentration factor at the notch root.[31] The FE analysis was continued till the stress redistribution across the notch throat plane attained a steady-state condition. The stress redistribution was considered to attain steady-state condition when the creep strain in the material at the notch throat plane reached the elastic strain, as stated by Calladine.[32]

The axial stress distributions across the notch throat plane after attaining the steady state considering 2D axisymmetric and 3D analysis are shown in Figure 3. It is interesting to note that the stress distribution after attaining the steady state was found not to be significantly affected by the types of analysis used for the simulation (Figure 3). Considering this fact, further detailed FE analysis has been carried out using 2D axisymmetric model only.

III. RESULTS AND DISCUSSION

A. *Creep Rupture Life of the Steels in the Presence of Notch*

Creep tests were carried out on smooth specimens over the stress range 90 to 300 MPa and notched specimens at the stresses in the range 110 to 230 MPa, 873 K (600 °C). The net applied stress (σ_{net}) at notch throat plane was same as that of applied stress (σ) as in the case of smooth specimen. The variations of steady-state creep rate as a function of applied stress for smooth specimens of the steels are shown in Figure 4(a). All the steels exhibited power-law relationship between steady-state creep rate and stress, except for the 2.25Cr-1Mo steel at higher stresses showing power-law breakdown. The variation of Percent elongation of the steels as a function of rupture life is shown in Figure 4(b). The 2.25Cr-1Mo steel possessed higher ductility than the 9Cr-steels. The variation of creep rupture lives of the steels under uniaxial (smooth specimen) and multiaxial (notched specimen) conditions is shown in Figures 5(a), (b) and (c), respectively, for the 2.25Cr-1Mo, 9Cr-1Mo,

Table II. Mechanical Properties of the Steels Obtained from Tensile and Creep Tests on Smooth Specimens

	Tensile Properties			Uniaxial Creep Properties	
Material\Element	Yield Stress (MPa)	K	n'	A ($MPa^{-n}\ h^{-1}$)	n
2.25Cr-1Mo Steel	290	474.24	0.073	9.17×10^{-17}	6.02
9Cr-1Mo Steel	310	445.65	0.049	1.27×10^{-21}	8.34
Mod. 9Cr-1Mo Steel	350	489.78	0.048	3.57×10^{-33}	12.92

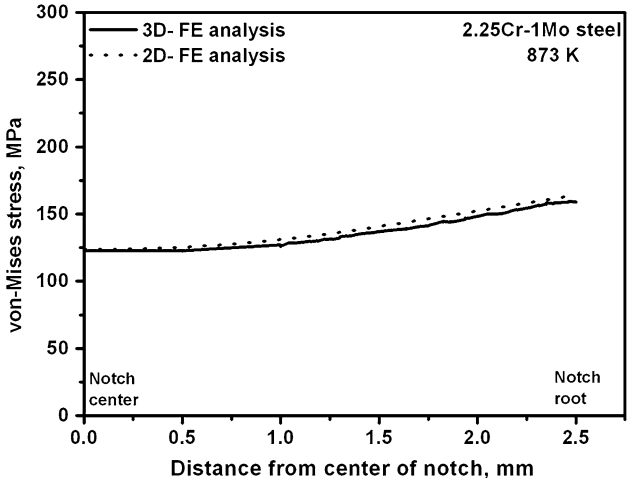

Fig. 3—Comparison of stress distribution across the notch throat plane considering 2D and 3D FE analysis.

and modified 9Cr-1Mo steels. The power-law breakdown in 2.25Cr-1Mo steel is also reflected in the variation of rupture life with stress, Figure 5(a). The creep rupture lives of the steels in the presence of notch (t_{rn}) were found to be higher than those of the smooth specimens (t_{rp}), exhibiting strengthening in the presence of notch in all the steels, Figure 5.

The rupture life of notched specimen increased with decrease in net applied stress and obeyed a power-law relation ($t_r = M'\sigma^{m'}$) as in the case of smooth specimens, where M' and m' are the stress coefficient and the stress exponent, respectively. Stress sensitivity of rupture life of the steels decreased in the presence of notch, and the decrease was relatively more for modified 9Cr-1Mo and least for 2.25Cr-1Mo steel. The extents of strengthening in the presence of notch in the different steels as functions of net applied stress and rupture life of smooth specimen are shown in Figures 6 and 7, respectively. The extent of strengthening of the steels in the presence of notch was found to increase in the order of 2.25Cr-1Mo, 9Cr-1Mo, and modified 9Cr-1Mo steels. The increase in strengthening was comparable for the 9Cr-Mo and 2.25Cr-1Mo steels. However, significant increase in strengthening was observed in modified 9Cr-1Mo steel. Eggeler *et al.*[4] studied the effect of notch on creep behavior of 9Cr-1Mo steel and observed strengthening in the steel. The strengthening effect was found to decrease with the decrease in applied stress and increase in rupture life for all the steels, as depicted by decrease in slopes of plots in Figures 6 and 7 with decrease in stress and increase in rupture life, respectively, and tend to saturate at lower applied stress and higher rupture lives.

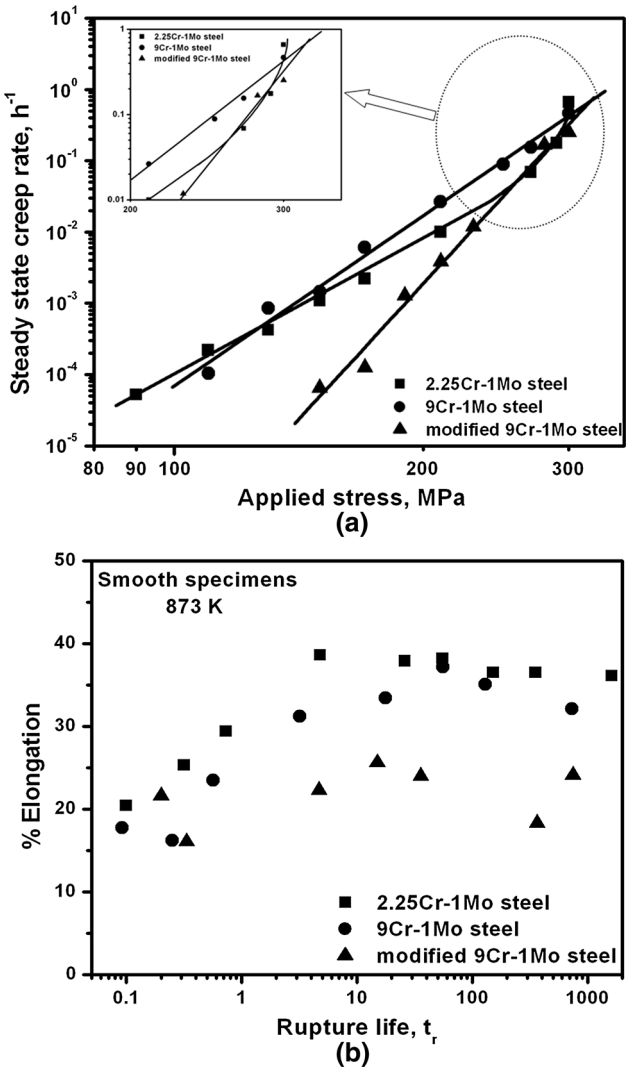

Fig. 4—Variations of (*a*) steady-state creep rate with applied stress and (*b*) percent elongation with rupture life for smooth specimen of the steels.

Studies carried out by Dyson *et al.*[33] on notched specimens showed notch strengthening in of Nimonic 80A superalloy. Al-Faddagh *et al.*[9] and Al-Abed *et al.*[17] also reported similar observations of notch strengthening for 2.25Cr-1Mo steel. However, Ng *et al.*[34] reported that the 0.5Cr-0.5Mo-0.25V steel (tempered bainitic structure) showed notch strengthening for shallow notches and tendency toward notch weakening for sharper notches. Notch strengthening has also been observed in modified 9Cr-1Mo steel by Wasmer *et al.*[16] Variations of creep rupture ductility

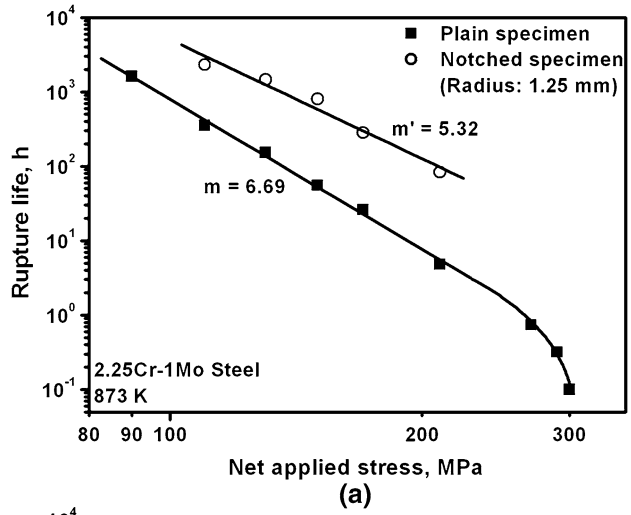

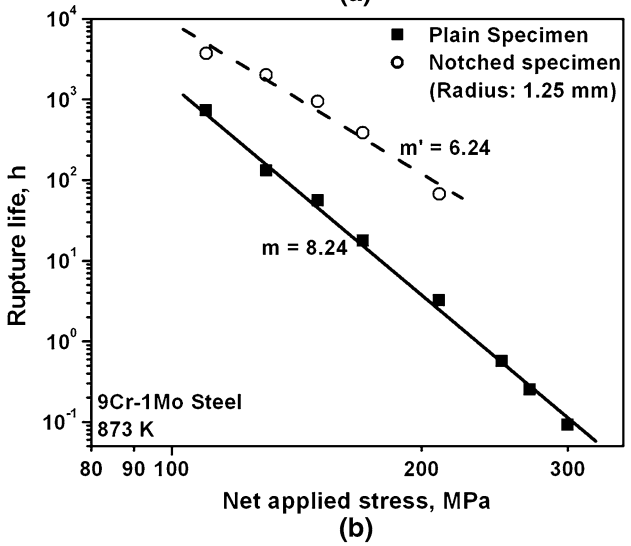

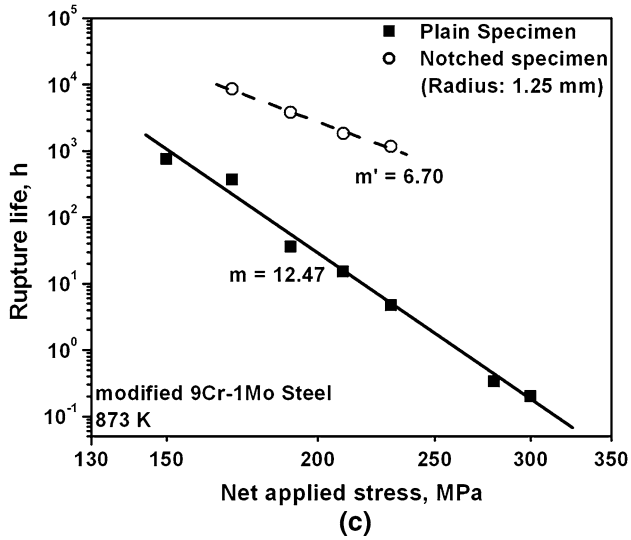

Fig. 5—Variation of creep rupture life as a function of net applied stress for (*a*) 2.25Cr-1Mo, (*b*) 9Cr-1Mo, and (*c*) modified 9Cr-1Mo steels.

of the steels (Percent reduction in area) in the presence of notch as a function of rupture life are shown in Figure 8 and compared with those of smooth specimen.

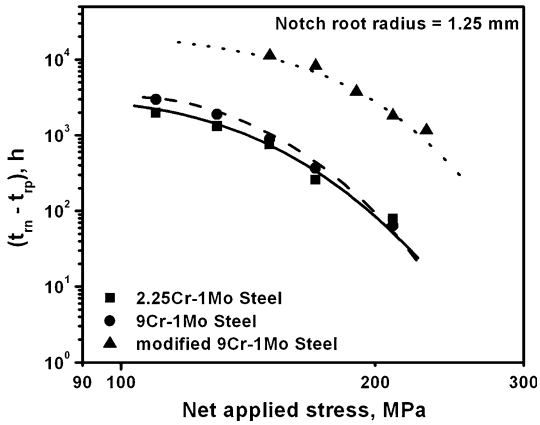

Fig. 6—Variations of notch strengthening ($t_{rn} - t_{rp}$) as a function of net applied stress for 2.25Cr-1Mo, 9Cr-1Mo, and mod. 9Cr-1Mo steels.

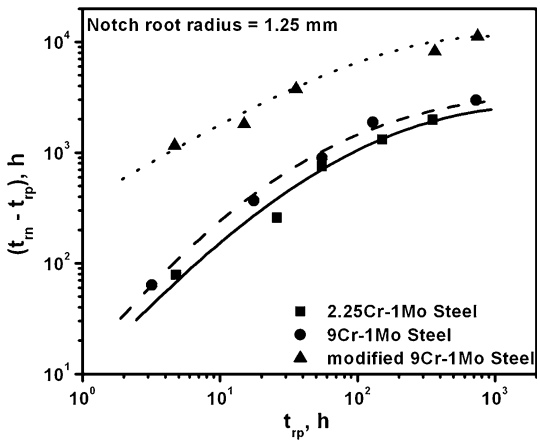

Fig. 7—Variations of notch strengthening ($t_{rn} - t_{rp}$) as a function of rupture life of smooth specimen for 2.25Cr-1Mo, 9Cr-1Mo, and mod. 9Cr-1Mo steels.

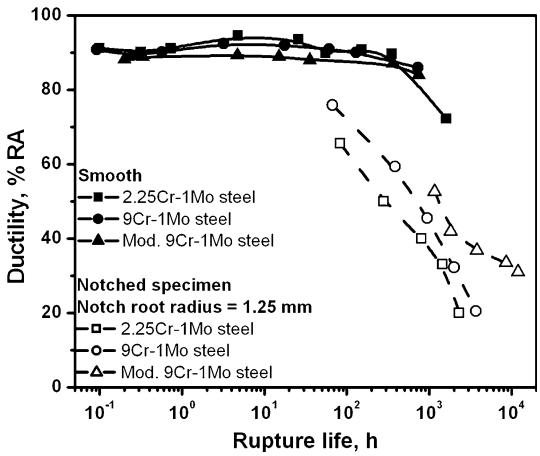

Fig. 8—Variations of creep ductility for plain and notched specimen for the steels.

The presence of notch decreased the creep rupture ductility of the steels significantly. The 2.25Cr-1Mo steel suffered more reduction in ductility in the presence of notch than the other two steels.

B. *Fracture Behavior of the Steels in the Presence of Notch*

Predominantly transgranular dimple failure was observed in the notched specimens of the steels at relatively higher applied stresses (Figures 9(a) and (b)), as in the smooth specimens (Figure 10). Shear lip, resulting in cup and cone type of failure, caused by final mechanical instability at the notch root region was observed, Figure 9(a). This indicated that the failure began at the central location of the notched specimen and propagated toward the notch root. Width of the shear lip zone was found to decrease with decrease in applied stress. The shape and size of the dimples in the failed notched specimens was found to depend on the applied stress and the location in the failed surface. Dimples around the central location of the notch throat plane were relatively bigger in size and deeper (Figure 11(a)) than those near to the notch root (Figure 11(b)). This indicates that the voids at the central location of notch throat would have grown appreciably by stress perpendicular to it leading to cup and cone type of fracture at relatively higher stresses. At relatively lower applied stresses, evidences of intergranular creep failure were also observed in 2.25Cr-1Mo at close to notch root, Figure 12. Eggeler *et al.*[4] have reported intergranular creep cavitation at the notch root for relatively lower applied stresses, suggesting a cross over of fracture mode for relatively lower stresses which may lead to notch weakening kind of behavior in the P9 steel. The studies carried out on alloy X-750 by Pandey *et al.*[5] showed notch strengthening in the material for the testing conditions. They observed that the crack initiation site moved systematically from notch center at high stresses toward the notch root at relatively lower stresses. For the notch root radius of 1.25 mm and over the stress range investigated, relatively less extent of creep cavitation was observed in the 9Cr-1Mo and modified 9Cr-1Mo steels. This indicates that these steels are more resistant to creep cavitation under multiaxial state of stress than the 2.25Cr-1Mo steel. Further, creep cavitation of exposed grain boundary facets has been studied employing SEM. The grain boundary facets with creep cavities were exposed by breaking the creep tested un-failed notch under impact load at liquid nitrogen temperature. Grain boundaries weakened in the presence of creep cavities provide easy path for intergranular crack propagation over that of the intragranular cleavage, resulting in two different fracture appearances, extent of which depends on the prior creep cavitation. The state of intergranular creep cavitations in the steels near to the notch root is shown in Figure 13. The propensity for creep cavitation under multiaxial state of stress near the notch root was found to be in the decreasing order of 2.25Cr-1Mo, 9Cr-1Mo, and modified 9Cr-1Mo steel.

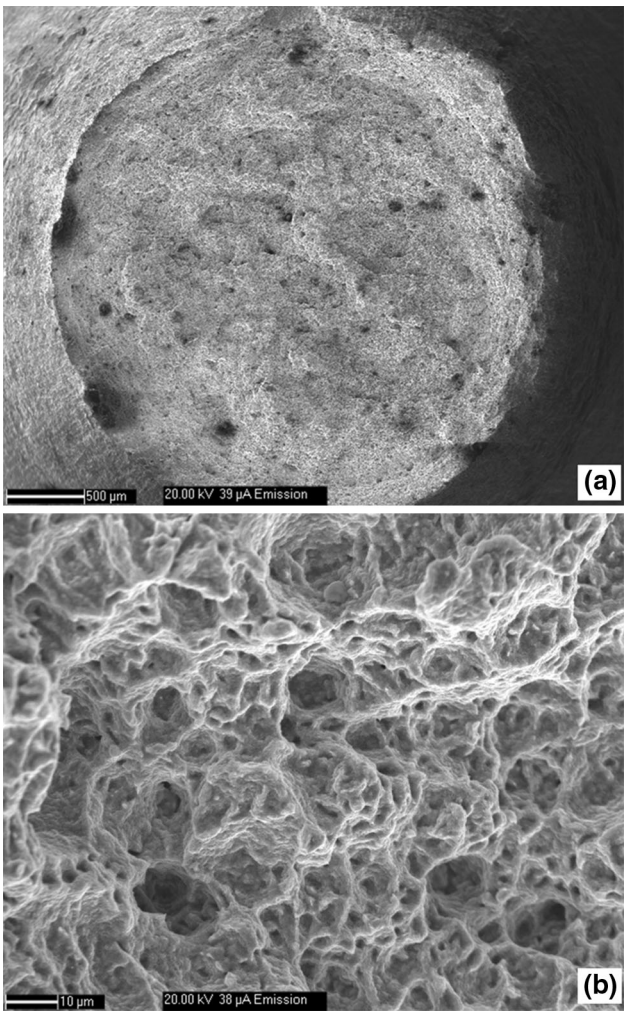

Fig. 9—(*a*) Typical cup and cone fracture with (*b*) dimpled ductile fracture appearance observed in notched specimen at relative higher stresses (210 MPa, 873 K) in 2.25Cr-1Mo steel.

C. *FE Analysis of Stress Distribution Across the Notch Throat Plane*

The steels under investigation exhibited notch strengthening under creep conditions, extent of which was found to depend on the material. Finite element analysis of stress distribution across the notch throat

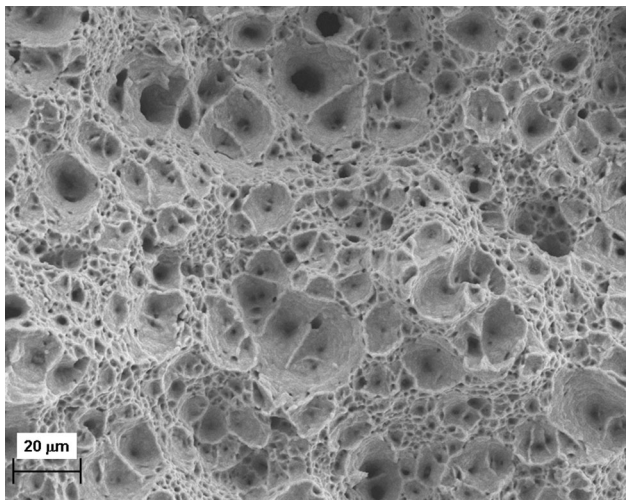

Fig. 10—Typical dimpled ductile fracture appearance observed in smooth specimen of 2.25Cr-1Mo steel creep tested at 150 MPa.

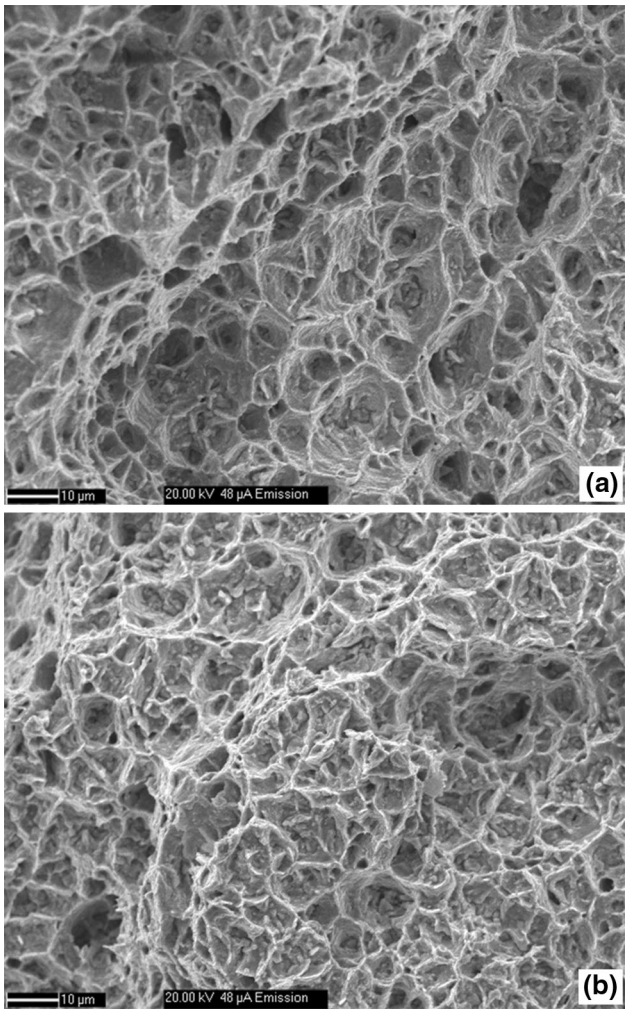

Fig. 11—(*a*) Relatively deep dimpled fracture at the central region of notch throat plane (*b*) relatively shallow dimpled fracture at the notch root region of notch throat plane, in notched specimen at relative lower stresses (130 MPa, 873 K) in 9Cr-1Mo steel.

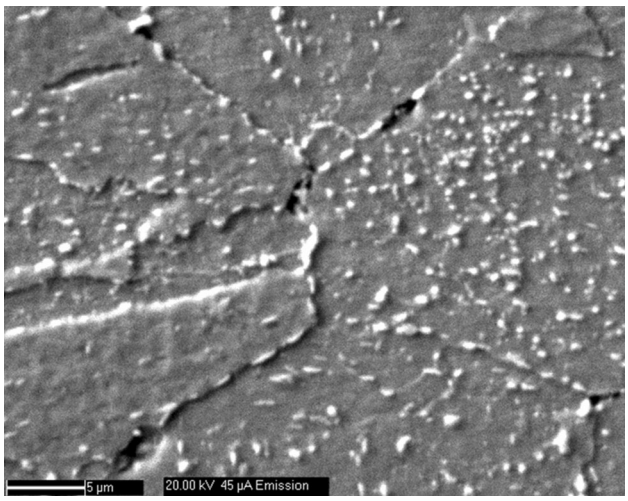

Fig. 12—Intergranular creep cavitation observed in notched specimen of 2.25Cr-1Mo steel creep tested at 130 MPa and 873 K.

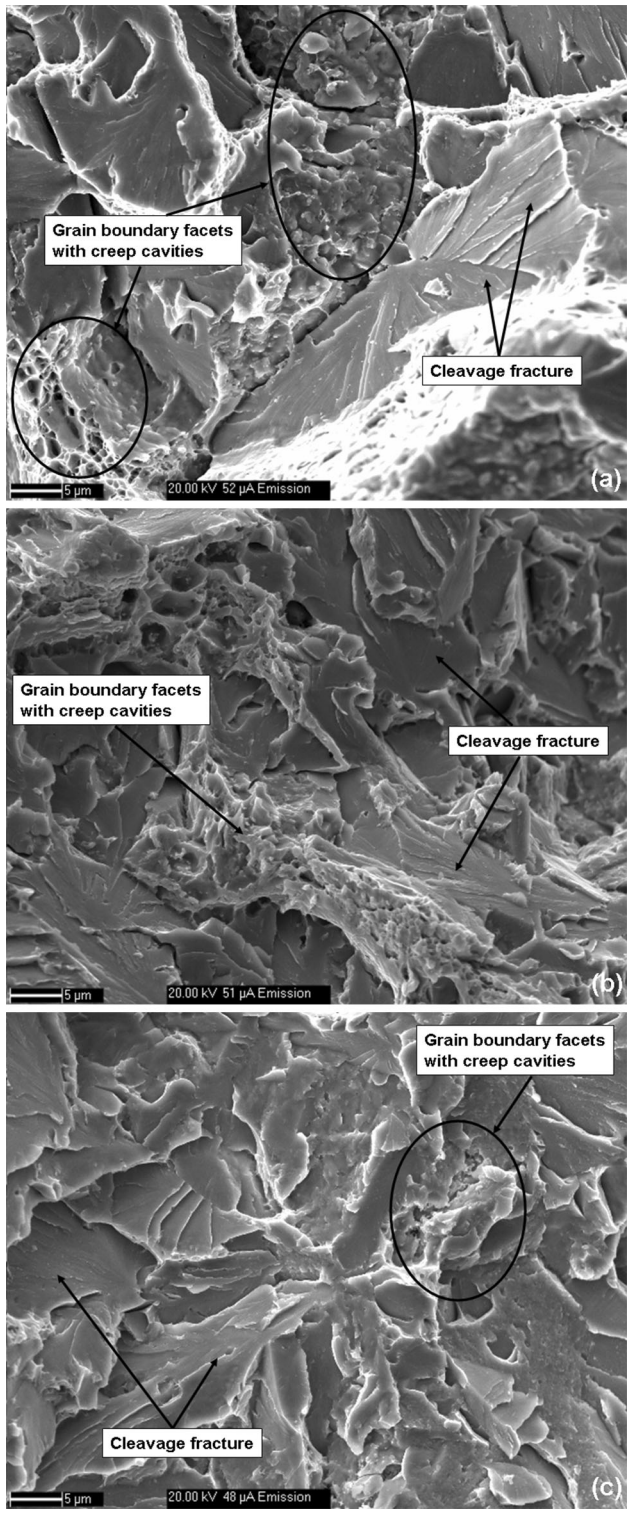

Fig. 13—SEM micrograph revealing creep cavities on grain facets, as exposed by breaking of creep exposed notched specimen at liquid nitrogen temperature for (*a*) 2.25Cr-1Mo (110 MPa), (*b*) 9Cr-1Mo (110 MPa), and (*c*) modified 9Cr-1Mo steels (190 MPa and 873 K).

plane during creep exposure was carried out to understand the difference in notch strengthening of the materials. The FE analysis was carried out on incorporating elastic–plastic-creep behavior of the materials.

1. *Distribution of von-Mises stress on initial loading*

On initial loading under multiaxial state of stress, the material will under go elastic deformation followed by plastic deformation. Von-Mises yield criterion has been used for onset of yielding in the steels during loading. Von-Mises stress under multiaxial state of stress is defined as

$$\sigma_{vm} = \sqrt{\frac{(\sigma_1 - \sigma_2)^2 + (\sigma_2 - \sigma_3)^2 + (\sigma_3 - \sigma_1)^2}{2}}$$

where σ_1, σ_2, and σ_3 are the maximum, intermediate, and minimum principal stresses, respectively. The distribution of von-Mises stress distribution across the notch throat plane for notch root radius of 1.25 mm for the steels immediately after loading is shown in Figure 14. The axial stress at the central region of notch throat plane was significantly lower than that of net applied stress (210 MPa). The von-Mises stress, governing the yielding in material, was higher than the yield stress for 2.25Cr-1Mo (290 MPa) and 9Cr-1Mo (310 MPa) steels at the notch root region resulting in localized yielding. Localized yielding at the notch root region resulted in decrease in stress at the notch root for 2.25Cr-1Mo and 9Cr-1Mo steels. However, for modified 9Cr-1Mo steel, stress concentration at the notch root was lower that yield stress (350 MPa) resulting in no reduction in the developed stresses. It is interesting to note that even after localized yielding at the notch root, the stresses experienced were found to be higher than that of net applied stress (210 MPa) for all the steels, Figure 14. Uniaxial creep tests were carried out up to 300 MPa based on the stresses developed in the notched specimens.

2. *Distribution of stresses during creep deformation*

Stress redistribution across the notch during creep exposure has been reported by several investigators.[12–15] The difference in creep rates across the notch due to change in diameter leads to stress redistribution across the notch throat plane during creep exposure. As creep deformation takes place, regions of high stress shed load to the regions of lower stresses due to the high stress sensitivity of creep deformation rate. Under creep condition, stress redistribution across the notch was found to change with creep exposure and approached to a steady state. The stresses across the notch especially across the notch throat plane were found to vary in a complex way. The axial stress was found to be significantly higher at the notch root than that around the center of notch throat plane after elastic/elastic–plastic deformation (axial stress after steady state for all the steels). With creep exposure, the axial stress at the center of notch throat plane increased, whereas it decreased at the notch root (Figure 15). The steady-state distribution of axial stress showed a maximum between the center of notch and notch root and had a value higher than the net applied stress.

The 2.25Cr-1Mo steel exhibited power-law breakdown at relatively higher stresses, Figure 4(a). However, the 9Cr-steels were found to obey power-law relation even at higher stresses. The higher stress exponent due to power-law breakdown in case of 2.25Cr-1Mo steel would result in accelerated localized creep deformation around the notch root. The stress distribution at the notch root with creep exposure for the steels at the net applied stress of 210 MPa is shown in Figure 16. It is interesting to note that the time required for the stress redistribution to attain the steady state was only a small fraction of total rupture life. The stress around the notch root redistributes quickly to a value below the power-law breakdown stress. Hence, it is expected that the Norton's law used for the 2.25Cr-1Mo steel is adequate to depict the material's behavior under multiaxial state of stress, and the power-law breakdown would not had affect the notch strengthening behavior of the steel appreciably.

The distributions of steady-state axial (maximum principal) stress considering both elastic-creep and elastic–plastic-creep behavior of 2.25Cr-1Mo steel at a net applied stress of 210 MPa across the notch throat

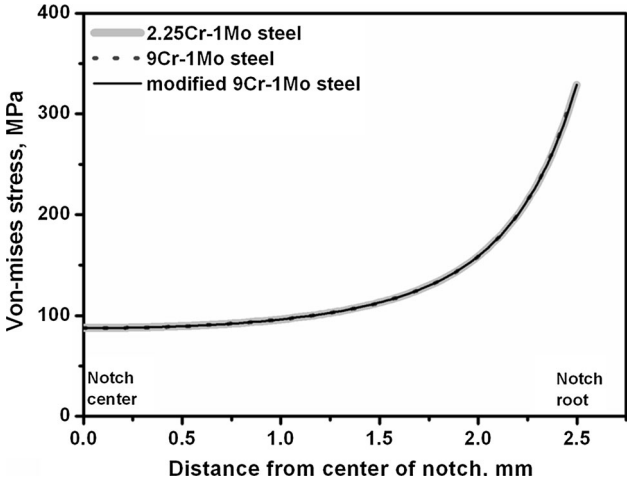

Fig. 14—Variations of von-Mises stress across the notch throat plane for all the steels after elastic/elastic–plastic deformation at 210 MPa and 873 K.

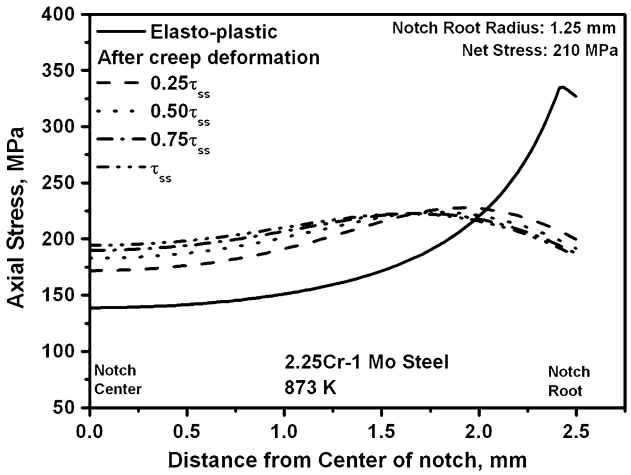

Fig. 15—Redistribution of axial stress across the notch throat plane as a function of creep exposure (τ_{ss} is the time to reach steady state).

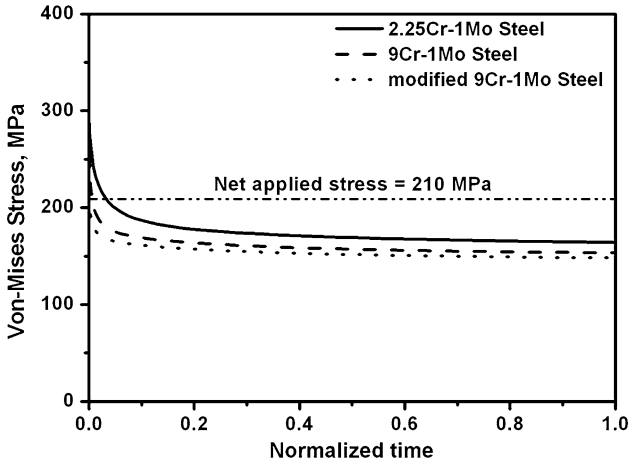

Fig. 16—Redistribution of von-Mises stress at the notch root as a function of creep exposure for different steels at 210 MPa.

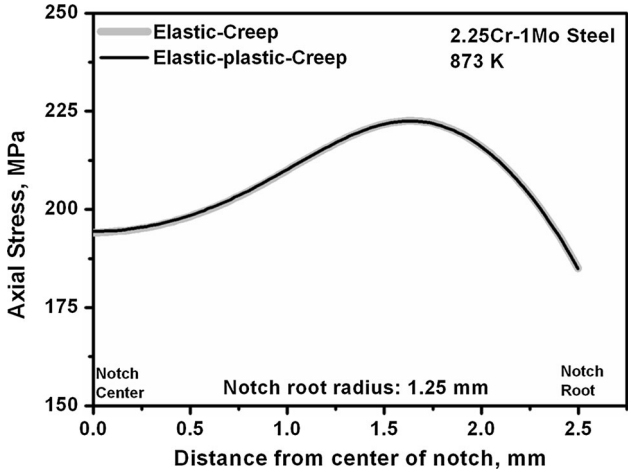

Fig. 17—FE analysis of axial stress distribution across the notch throat plane considering elastic-creep and elastic–plastic-creep behavior of 2.25Cr-1Mo steel at 210 MPa and 873 K (600 °C).

plane are shown in Figure 17. It can be concluded that localized plastic deformation at the notch root does not play significant role in the distribution of stresses across the notch throat plane during creep exposure.

3. *Creep cavitation in the steels in presence of Notch*

Creep cavitation in materials occurs by cavity nucleation, their growth, and final fracture. Since the nucleation of creep cavity occurs due to constrained deformation across the discontinuities at the grain boundary, the grain boundary sliding which is controlled by plastic deformation of the matrix, von-Mises stress, plays a major role in creep cavity nucleation.[35] However, stability of the nucleated creep cavities is decided by the maximum principal stress as the critical cavity size r_c which can avoid the sintering governed by $r_c = 2\gamma_c/\sigma_1$, where γ_c is the surface energy and σ_1 is the maximum principal stress. For the growth of existing creep cavity, it has to attain the critical size otherwise the cavity will sinter. The nucleated stable creep cavity

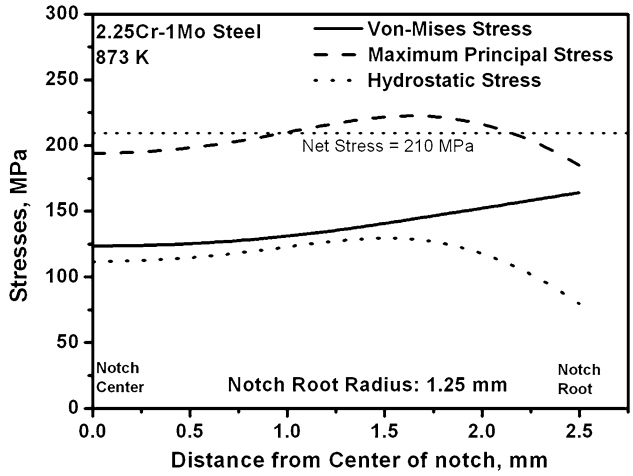

Fig. 18—Distribution of von-Mises, maximum principal, and hydrostatic stresses across the notch throat plane after attaining the steady state.

can grow basically by two mechanisms: (i) plasticity-controlled growth[36] and (ii) stress-directed flow of atoms (diffusive growth).[37] Cavity can grow in the presence of hydrostatic stress. Cavity growth by plasticity controlled by von-Mises stress occurs as a result of creep deformation of the matrix surrounding the grain boundary cavity in the absence of vacancy flux.[38] The von-Mises stress will assist the cavity growth by inducing plasticity, whereas cavity growth by stress-directed flow of atom will be controlled by maximum principal stress. The cavity growth at high temperatures can also be driven by the hydrostatic component of the stress state, as in the case of high-temperature ductile fracture.

Creep deformation and cavitation behavior of the Cr-Mo steels under multiaxial state of stress have been assessed based on the distribution of the von-Mises, principal, and hydrostatic stresses across the notch throat plane. Variations of the steady-state von-Mises, maximum principal, and hydrostatic stresses across the notch throat plane for 2.25Cr-1Mo steel are shown in Figure 18. The von-Mises stress was found to remain below the net applied stress and increased toward notch root. Maximum principal stress was found to be lower than net applied stress at the center and root of notch and showed a maximum value which was more than the net applied stress. The behavior of hydrostatic stress under steady-state condition across the notch throat plane was similar to that of principal stress, but the maximum value of the hydrostatic stress remained below the net stress. Similar variations in different components of stresses have been observed for other two steels.

The decrease in von-Mises stress below the net applied stress after stress redistribution leads to the creep strengthening in the steels in the presence of notch (Figure 5).[10] Figure 6 revealed that the extent of strengthening in the presence of notch decreased with decrease in net applied stress and tends to saturate at relatively lower applied stresses. The decrease in steady-state von-Mises stresses compared to that in the smooth specimen (net applied stress) across the notch throat

plane is shown in Figure 19(a) for different net applied stresses. The reduction in von-Mises stress across the notch throat plane decreased with net applied stress, indicating that the extent of strengthening in the presence of notch decreases with decrease in applied stresses. The difference of maximum principal stress with respect to net applied stress across the notch throat plane at different applied stresses is shown in Figure 19(b). The maximum principal stress across the notch throat plane was less than the net applied stress both in the notch central and root regions. The reduction in maximum principal stress became less with decrease in applied stress. At regions close to notch root, the maximum principal stress was more than the net applied stress, and the increase was less for lower applied stresses. Presence of high principal stress coupled with relatively higher von-Mises stress near to the notch root region is expected to nucleate and stabilize the intergranular creep cavity. However, under higher net applied stresses resulting in relative less creep rupture life, nucleated creep cavity would have little time to grow by diffusive transfer of atoms from cavity surface to grain boundary for inducing creep cavitation.

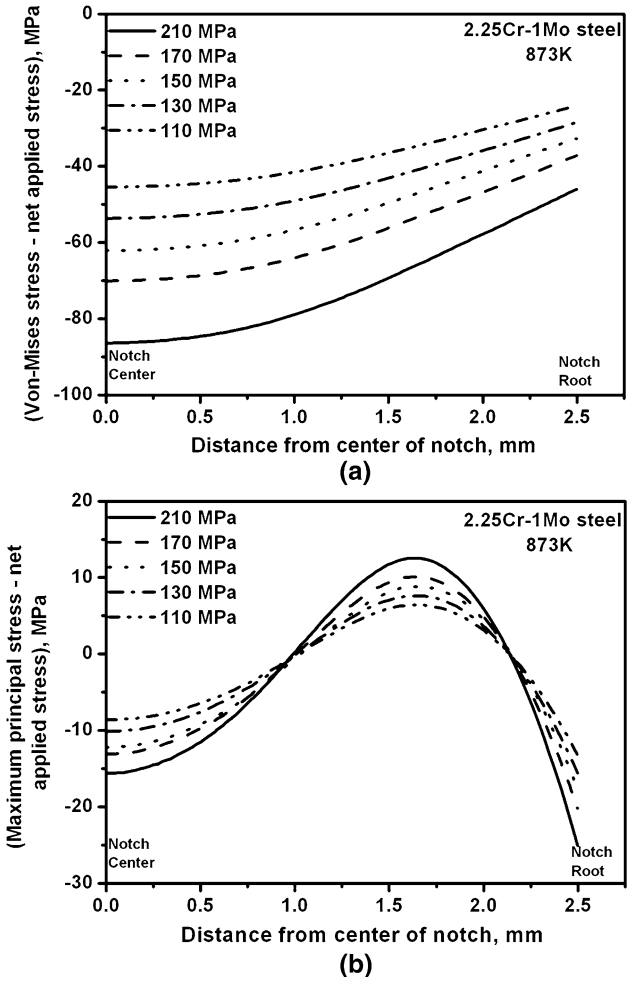

Fig. 19—Variation of difference in (*a*) von-Mises and (*b*) maximum principal stresses with respect to net applied stress across the notch throat plane for different net applied stresses.

Thus, predominantly ductile dimple failure in notch specimens was observed at higher applied stresses (Figures 9 and 11). At lower applied stresses causing

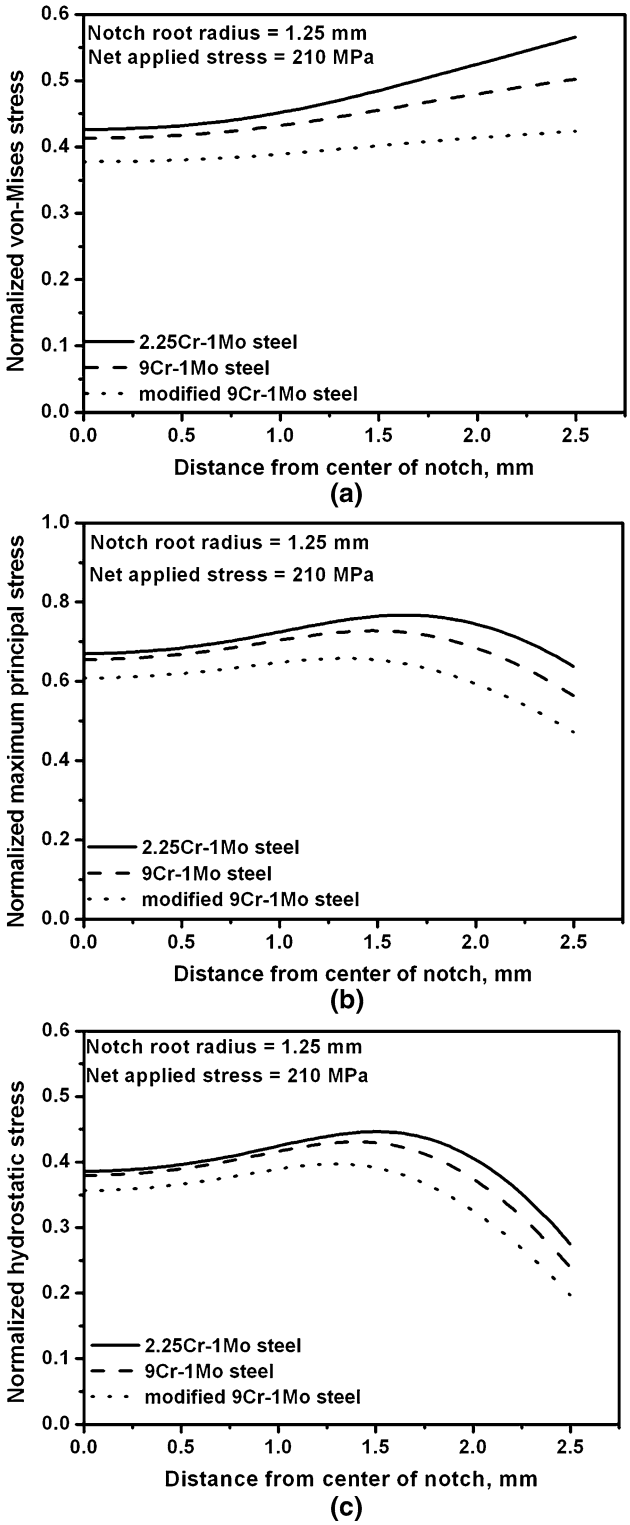

Fig. 20—Distribution of normalized (*a*) von-Mises, (*b*) maximum principal, and (*c*) hydrostatic stresses across the notch throat plane after attaining the steady state in 2.25Cr-1Mo, 9Cr-1Mo, and modified 9Cr-1Mo steels.

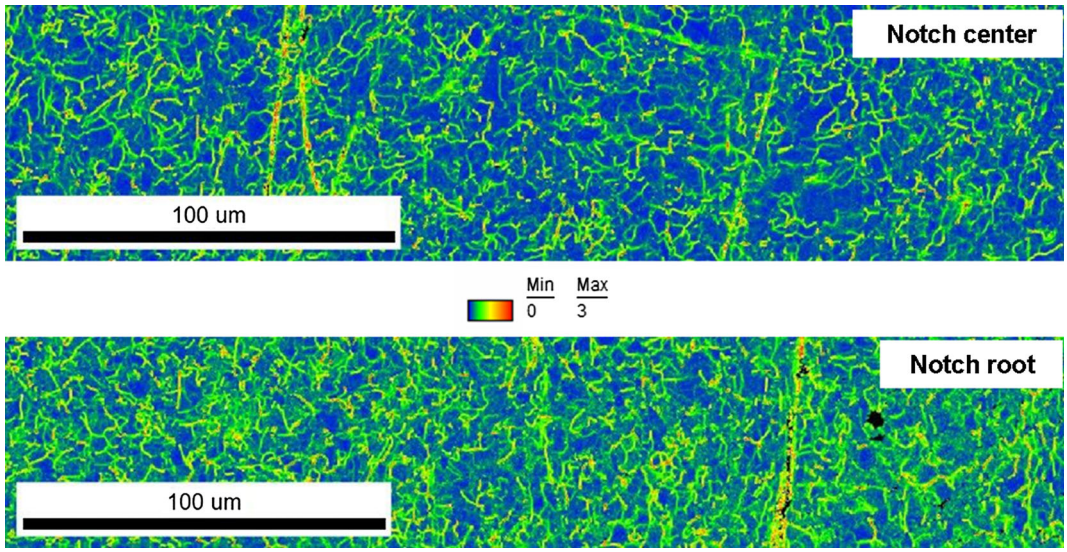

Fig. 21—Kernel average misorientation maps at center and root regions of notch for 2.25Cr-1Mo steel creep tested at 110 MPa and 873 K (600 °C).

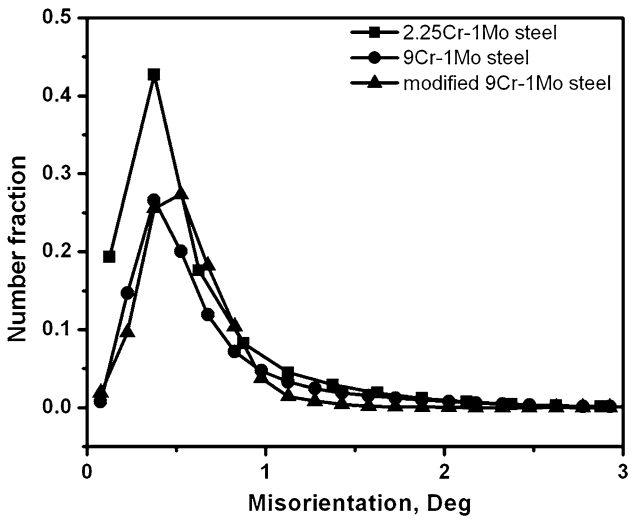

Fig. 22—Number fraction of KAM at the notch root of 2.25Cr-1Mo, 9Cr-1Mo, and modified 9Cr-1Mo steels creep tested at 170 MPa, 873 K (600 °C).

relatively longer creep rupture life, evidences of intergranular creep cavitation were observed near to the notch root region (Figure 12).

4. *Material dependency of Notch strengthening*

The presence of notch was found to increase the creep rupture life of the steels (Figure 5). The extent of strengthening was comparable for the 2.25Cr-1Mo and 9Cr-1Mo steels. However, the modified 9Cr-1Mo steel exhibited more extensive strengthening than that of the other two steels (Figure 6). To assess the different extent of notch strengthening in different steels, FE analysis of stress distribution across the notch throat plane was carried out on incorporating the tensile and creep deformation properties of the individual steels.

The redistribution of von-Mises stress at the notch root with creep exposure for different steels is shown in Figure 16. The time for redistribution has been normalized with the time to reach steady-state stress distribution for the steels. The stresses relaxed with creep exposure at different rates and to a different extents depending upon the materials. The redistribution was relatively faster for modified 9Cr-1Mo steel and slowest for 2.25Cr-1Mo steel, because of higher stress sensitivity of creep deformation in modified 9Cr-1Mo steel (n = 12.92) than that in 2.25Cr-1Mo (n = 6.02) and 9Cr-1Mo steels (n = 8.34). This is reflected in the difference in the steady-state variation of maximum principal, von-Mises, and hydrostatic stress variations across the notch throat plane. The variations of maximum principal, von-Mises, and hydrostatic stresses normalized with respect to yield stress of individual steel are shown in Figure 20. The normalized stresses were found to be in the increasing order of modified 9Cr-1Mo, 9Cr-1Mo, and 2.25Cr-1Mo steel. Higher stresses across the notch throat plane in 2.25Cr-1Mo steel results from the lack of stress redistribution (Figure 16) than in other two steels. This implies that at a given net applied stress 2.25Cr-1Mo steel would spend most of its life time in higher stress than in modified 9Cr-1Mo steel, resulting in lower notch strengthening (Figure 6).

In order to understand the creep deformation and damage across the notch throat plane, EBSD was carried out on the un-failed notch of the steels. The KAM map has been successfully used to evaluate localized plastic strain in materials.[39–41] Kernel average misorientation (KAM) maps (calculated on the basis of first nearest neighbor) obtained at the center and root regions of the notch for the 2.25Cr-1Mo steel creep tested at 110 MPa are shown in Figure 21, showing higher extent of misorientation in the notch root region than that in the notch central region. Higher KAM values in the grains correspond to higher local misori-

entations (*i.e.*, higher creep deformation). It is clearly evident that the creep deformation is relatively more at the notch root as compared to the center of notch. The distribution of KAM value at the notch root region for the 2.25Cr-1Mo, 9Cr-1Mo, and modified 9Cr-1Mo steels is shown in Figure 22. The peak of the KAM value was found to be in the decreasing order of 2.25Cr-1Mo, 9Cr-1Mo, and modified 9Cr-1Mo steel. However, the peak value of KAM was found to be at the same misorientation angle for all the steels. This indicates that 2.25Cr-1Mo steel has experienced more deformation as compared to the other two steels.

IV. CONCLUSIONS

The following conclusions have been drawn based on the studies on the effect of multiaxial state of stress introduced by notch with root radius of 1.25 mm on creep rupture strength of 2.25Cr-1Mo, 9Cr-1Mo, and modified 9Cr-1Mo steel, creep tested at 873 K (600 °C) over a stress range 110 to 230 MPa and distribution of stresses across the notch based on finite element analysis:

1. Multiaxial state of stress introduced incorporating notch in uniaxial specimen led to increase in creep rupture life of the steels. The increase in creep rupture life decreased with decrease in applied stress and tends to saturate at lower applied stress.
2. The increase in creep rupture strength under multiaxial state of stress was comparable for 2.25Cr-1Mo and 9Cr-1Mo steels whereas significantly more for modified 9Cr-1Mo steel.
3. Creep ductility of the steels decreased under multiaxial state of stress, which became more significant at lower applied stress. The reduction in creep rupture strength was more for 2.25Cr-1Mo steel and less for modified 9Cr-1Mo steel.
4. Under the investigated multiaxial state of stress, the steels failed predominantly in ductile mode with some evidences of intergranular creep failure especially on long-term creep exposure. The 2.25Cr-1Mo steel was more prone to intergranular creep cavitation than both the 9Cr-steels.
5. The von-Mises stress across the notch throat plane was less than the net applied stress and progressively increased from notch center to notch root. The maximum principal stress showed a maximum value between notch center and root, and the maximum value was more than net applied stress.
6. The reduction in von-Mises stress across the notch throat plane under multiaxial state of stress increased the creep rupture life of the steels. Higher reduction led to more creep rupture strength in modified 9Cr-1Mo steel than that in other two steels. The lower extent of von-Mises stress reduction with decrease in applied stress led to tendency of saturation at lower stress.
7. Presence of relatively higher maximum principal stress close to the notch root region was found to promote intergranular creep cavitation at notch root region. Relatively higher maximum principal stress in 2.25Cr-1Mo than that in the 9Cr-steels revealed higher susceptibility to intergranular creep cavitation in 2.25Cr-1Mo steel than in 9Cr-1Mo and modified 9Cr-1Mo steels.

ACKNOWLEDGMENTS

The authors are grateful to Dr. P. R. Vasudeva Rao, Director, Indira Gandhi Centre for Atomic Research (IGCAR); Dr. T. Jayakumar, Director, Metallurgy and Materials Group, IGCAR; and Dr. A.K. Bhaduri, AD, MDTG for their constant encouragement and support. The authors are also thankful to Ms. S. Panneerselvi for his help in SEM fractography.

REFERENCES

1. K. Laha, K.S. Chandravathi, P. Parameswaran, and K.B.S. Rao: *Metall. Mater. Trans. A*, 2009, vol. 40A, pp. 386–97.
2. B.K. Choudhary, S. Saroja, K.B.S. Rao, and S.L. Mannan: *Metall. Mater. Trans. A*, 1999, vol. 30A, pp. 2825–34.
3. D.J. Smith, N.S. Walker, and S.T. Kimmins: *Int. J. Press. Vess. Piping*, 2003, vol. 80, pp. 617–27.
4. G. Eggeler, W. Tato, P. Jemmely, and B. de Mestral: *Scripta Metall. Mater.*, 1992, vol. 27, pp. 1091–96.
5. M.C. Pandey, A.K. Mukherjee, and D.M.R. Taplin: *J. Mater. Sci.*, 1985, vol. 20, pp. 1201–06.
6. Y.P. Jiang, W.L. Guo, and Z.F. Yue: *Comp. Mater. Sci*, 2007, vol. 38, pp. 653–59.
7. S. Goyal, K. Laha, C.R. Das, and S. Panneer: Selvi, and M.D. Mathew*Metall. Mater. Trans. A*, 2014, vol. 45A, pp. 619–32.
8. P.S. Webster and A.C. Pickard: *J. Strain Anal.*, 1987, vol. 22, pp. 145–53.
9. K.D. Al-Faddagh, G.A. Webster, and B.F. Dyson: *Mechanical Behaviour of Materials IV*, J. Carlsson and N.G. Ohlson, eds., Pergamon Press, Oxford, 1984, pp. 289–95.
10. D. McLean, B.F. Dyson, and D.M.R. Taplin: in *The Fourth International Conference on Fracture*, vol. 1, D.M.R. Taplin, ed., University of Waterloo Press, Waterloo, 1977, pp. 325–62.
11. E.A. Davis and M.J. Manjoine: "Effect of Notch Geometry on Rupture Strength at Elevated Temperatures", ASTM STP 128, 1953, pp. 67–87.
12. D.R. Hayhurst and G.A. Webster: in *Techniques for Multiaxial Creep Testing*. D.J. Gooch and I.M. How, eds., Elsevier Applied Science, Amsterdam, 1986, pp. 137–75.
13. D. Wu, E.M. Christian, and E.G. Ellison: *J. Strain Anal.*, 1984, vol. 19, pp. 209–20.
14. D.R. Hayhurst and J.T. Henderson: *Int. J. Mech. Sci.*, 1977, vol. 19, pp. 133–46.
15. G. Eggeler and C. Wiesner: *J. Strain Anal.*, 1993, vol. 28, pp. 13–22.
16. K. Wasmer, F. Bilgari, and K.M. Nikbin: *European Conference on Fracture; ECF 14, Fracture Mechanics Beyond 2000*, 2002, pp. 553–62.
17. B. Al-Abed, R. Timmins, G.A. Webster, and M.S. Loveday: *Mater. High Temp.*, 1999, vol. 16, pp. 143–58.
18. A.A. Becker, T.H. Hyde, W. Sun, and P. Andersson: *Comp. Mater. Sci.*, 2002, vol. 25, pp. 34–41.
19. O. Kwon, C.W. Thomas, and D. Knowles: *Int. J. Press. Vess. Piping*, 2004, vol. 81, pp. 535–42.
20. H.K. Kim and H.J. Kim: *J. Mater. Sci.*, 2008, vol. 43, pp. 2602–10.
21. M.C. Pandey, A.K. Mukherjee, and D.M.R. Taplin: *J. Mater. Sci.*, 1985, vol. 20, pp. 1201–06.
22. B.J. Cane: *Proc. 5th Int. Conf. Fract. Cannes*, 1981, vol. 3, pp. 1285–93.

23. S. Goyal, K. Laha, K.S. Chandravathi, P. Parameswaran, and M.D. Mathew: *Phil. Mag.*, 2011, vol. 91, pp. 3128–54.
24. I.J. Perrin and D.R. Hayhurst: *Int. J. Press. Vess. Pip.*, 1999, vol. 76, pp. 599–617.
25. N. Bano, A.K. Koul, and M. Nganbe: *Metall. Mater. Trans. A*, 2014, vol. 45A, pp. 1928–36.
26. G.H. Edward and M.F. Ashby: *Acta Metall.*, 1979, vol. 27, pp. 1505–18.
27. K.J. Hsia, A.S. Argon, and D.M. Parks: *Mech. Mater.*, 1991, vol. 11, pp. 43–62.
28. K.J. Hsia, A.S. Argon, and D.M. Parks: *Mech. Mater.*, 1991, vol. 11, pp. 19–42.
29. D.R. Hayhurst, F.A. Leckie, and J.T. Henderson: *Int. J. Mech. Sci.*, 1977, vol. 19, pp. 147–59.
30. G.A. Webster, S.R. Holdsworth, M.S. Loveday, K. Nikbin, I.J. Perrin, H. Purper, R.P. Skelton, and M.W. Spindler: *Fat. Frac. Eng. Mater. Struct.*, 2004, vol. 27, pp. 319–42.
31. W.D. Pilkey and D.F. Pilkey: *Peterson's Stress Concentration Factors*, 3rd ed., Wiley, New York, 2008.
32. C.R. Calladine: *Proc. R Soc. Lond. A*, 1969, vol. 309, pp. 363–75.
33. B.F. Dyson and M.S. Loveday: *Proc. Creep in Structures, TUTAM Symp.* Pergamon Press, Oxford, pp. 406–21.
34. S.E. Ng, G.A. Webster and B.F. Dyson: in *Advances in Fracture Research, ICF-5*, D. Francois *et al.*, eds., Pergamon Press, Oxford, 1980, pp. 1275–83.
35. W.D. Nix, J.C. Earthman, G. Eggeler, and B. Ilschner: *Acta Metall.*, 1989, vol. 37, pp. 1067–77.
36. J.W. Hancock: *Met. Sci.*, 1976, vol. 10, pp. 319–25.
37. D. Hull and D.E. Rimmer: *Phil. Mag.*, 1959, vol. 4, pp. 673–87.
38. M.F. Ashby, C. Gandhi, and D.M.R. Taplin: *Acta Metall.*, 1979, vol. 27, pp. 699–729.
39. D. Peter, F. Otto, T. Depka, P. Nortershauser, and G. Eggeler: *Mat.-wiss. u.Werkstofftech*, 2011, vol. 42, pp. 493–99.
40. D. Kobayashi, M. Miyabe, Y. Kagiya, Y. Nagumo, R. Sugiura, T. Matsuzaki, and A.T. Yokobori, Jr.: *Strength Fract Complex*, 2011, vol. 7, pp. 157–67.
41. S. Mandal, A.K. Bhaduri, and V.S. Sarma: *J. Mater. Sci.*, 2011, vol. 46, pp. 275–84.